# Synthesis, Luminescence Properties, and Explosives Sensing with 1,1-Tetraphenylsilole- and 1,1-Silafluorene-vinylene Polymers

Jason C. Sanchez, Antonio G. DiPasquale, Arnold L. Rheingold,* and William C. Trogler*

*Department of Chemistry and Biochemistry, University of California at San Diego, 9500 Gilman Drive, La Jolla, California 92093-0358*

*Received August 14, 2007. Revised Manuscript Received October 3, 2007*

The syntheses, spectroscopic characterizations, and fluorescence quenching efficiencies of polymers and copolymers containing tetraphenylsilole- or silafluorene-vinylene repeat units are reported. These materials were prepared by catalytic hydrosilylation reactions between appropriate monomeric metallole alkynes and hydrides. Trimeric model compounds methyl(tetraphenyl)silole-vinylene trimer (**1**), methyl(tetraphenyl)silole-silafluorene-vinylene cotrimer (**2**), and methylsilafluorene-vinylene trimer (**3**) were synthesized to provide detailed structural and spectroscopic characteristics of the polymer backbone and to assess the extent of delocalization in the luminescent excited state. Poly(tetraphenylsilole-vinylene) (**4**), poly(tetraphenylsilole-silafluorene-vinylene) (**5**), and poly(silafluorene-vinylene) (**6**) maintain a regioregular *trans*-vinylene Si−C backbone with possible ground state $\sigma^*-\pi$ and excited state $\sigma^*-\pi^*$ conjugation through the vinylene bridge between metallole units. Fluorescence spectra of the polymers show an ∼13 nm bathochromic shift in $\lambda_{flu}$ from their respective model compounds. Molecular weights ($M_n$) for these polymers and copolymers are in the range of 4000–4500. Detection of nitroaromatic explosives by solution-phase fluorescence quenching of polymers **4**−**6** was observed with Stern−Volmer constants in the range of 400−20 000 for TNT, DNT, and picric acid (PA). A surface detection method for the analysis of solid particulates of TNT, DNT, PA, RDX, HMX, Tetryl, TNG, and PETN is also described for silafluorene-containing polymers. Polymer **6** exhibited detection for all the preceding types of explosive residues with a 200 pg $cm^{-2}$ detection limit for Tetryl. Polymers **4** and **5** exhibited only luminescence quenching with nitroaromatic explosives, revealing that the excited-state energy of the sensor plays a key role in the fluorescence detection of explosives.

## Introduction

Reliable detection of trace explosive materials has become a focal point in security screening methods. Applications such as minefield remediation,[1] crime scene investigations,[2] and counterterrorism activities (e.g., facility protection and personnel, baggage, and cargo screening[3]) are areas of concern. Instrumental techniques include gas chromatography coupled with mass spectrometry,[4] gas chromatography-electron capture detection,[2] surface-enhanced Raman spectroscopy,[5] mass spectrometry,[6] X-ray imaging, nuclear quadrupole resonance, thermal and fast neutron analysis, and ion mobility spectrometry.[7] Approaches have been adapted for both bulk and trace detection methods to analyze suspicious materials, personnel, and cargo. Cost, complexity, and robust portability are problematic for many of these methods.

Conventional spectroscopic and imaging techniques typically employ bulk or vapor phase sampling. As described in a previous report,[8] vapor sampling may be limited by the low volatility of many explosives at room temperature. Nitroaromatic explosives such as TNT have moderate vapor pressures ($7 \times 10^{-6}$ Torr at room temperature), but at low surface concentrations, the vapor concentration of TNT is significantly less than its equilibrium vapor pressure.[9] Explosives, such as RDX and HMX, have substantially lower vapor pressures ($5 \times 10^{-9}$ and $8 \times 10^{-11}$ Torr, respectively), which makes vapor detection of these compounds difficult.[10]

An alternative to vapor sampling is the chemical analysis of solid particulates that remain after the handling of explosive materials.[11] This includes colorimetric and fluorescence sensing devices that take advantage of human visual processing power, rather than instrumental evaluation.[12–14]

* Corresponding author. E-mail: wtrogler@ucsd.edu (W.C.T.); arnrhein@ucsd.edu (A.L.R.).

(1) Steinfeld, J. I.; Wormhoudt, J. *Annu. Rev. Phys. Chem.* **1998**, *49*, 203–232.
(2) Smith, K. D.; McCord, B. R.; McCrehan, W. A.; Mount, K.; Rowe, W. F. *J. Forensic Sci.* **1999**, *44*, 789–794.
(3) Rouhi, A. M. *Chem. Eng. News* **1997**, *75*, 14–22.
(4) Hakansson, K.; Coorey, R. V.; Zubarev, R. A.; Talrose, V. L.; Hakansson, P. *J. Mass. Spectrom.* **2000**, *35*, 337–346.
(5) Sylvia, J. M.; Janni, J. A.; Klein, J. D.; Spencer, K. M. *Anal. Chem.* **2000**, *72*, 5834–5840.
(6) Popov, I. A.; Chen, H.; Kharybin, O. N.; Nikolaev, E. N.; Cooks, R. G. *Chem. Commun.* **2005**, *15*, 1953–1955.
(7) Kolla, P. *Anal. Chem.* **1995**, *67*, 184A–189A.
(8) Toal, S. J.; Sanchez, J. C.; Dugan, R. E.; Trogler, W. C. *J. Forensic Sci.* **2007**, *52*, 79–83.
(9) Trogler, W. C. *Electronic Noses & Sensors for the Detection of Explosives*; Gardner, J. W., Yinon, J., Eds.; Kluwer Academic Publishers: Dordrecht, The Netherlands, 2004; p 39.
(10) Mostak, P. *Vapour and Trace Detection of Explosives for Anti-terrorism Purposes*; Krausa, M., Reznev, A. A., Eds.; Kluwer Academic Publishers: Dordrecht, The Netherlands, 2004; p 23.
(11) Committee on Assessment of Security Technologies for Transportation. *Opportunities to Improve Airport Passenger Screening with Mass Spectrometry*; National Academy of Sciences: Washington, D.C., 2003.
(12) Plexus Scientific Corporation. http://www.plexsci.com/expray.shtml (Accessed Nov 27, 2006).

10.1021/cm702299g CCC: $37.00 
Published on Web 11/21/2007

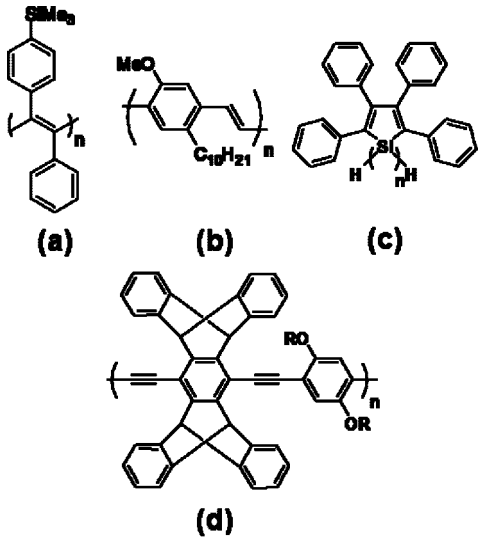


**Figure 1.** Conjugated fluorescent polymers for explosives detection: (a) polyacetylene PTMSDPA, (b) poly(*p*-phenylenevinylene) DP10-PPV, (c) 1,1-poly(tetraphenyl)silole, and (d) poly(*p*-phenylene-ethynylene).

The use of fluorescent polymers for the detection of explosive vapors and particulates has been adapted for both instrumental and visual imaging approaches (Figure 1).[14] Poly(tetraphenyl)siloles, in particular, have the advantage of ease of synthesis and their ability to semiselectively bind explosive analytes (Figure 1c).[15] Previous reports have demonstrated the ability of 1,1-poly(tetraphenyl)silole to image trace particulates of explosive materials in the solid state.[15d,8] However, no single polymer has been able to detect the entire range of common high explosives by a fluorescence quenching mechanism, in part because of the broad range of reduction potentials found among explosive materials. The use of a wide band gap polymer should create optimal energy overlap with a more extensive collection of explosive materials. However, there remain relatively few examples of stable conjugated polymers that emit in the UV-blue region of the spectrum.[16]

Siloles, such as silicon-containing 2,3,4,5-tetraphenylsilacyclopentadienes, are highly luminescent in the solid state.[17] Their unique photoelectronic properties arise from conjugation between the $\sigma^*$ orbitals of the bridging silicon and the $\pi^*$ orbital of the metallole butadiene fragment.[18] Silafluorene derivatives possess similar core electronic features but their biphenyl framework increases the band gap energy, allowing for UV-blue emission. Both metalloles have been studied as electron-transporting materials,[19] OLED materials[20] and inorganic polymer sensors.[15,8] Typical synthetic routes to metallole polymers include Suzuki,[21] Sonogashira,[22] and various coupling reactions[20a,23] through positions on the aromatic systems. There are only a few examples of metallole polymerization in the 1,1 positions (dehydrocoupling and Wurtz coupling) and only one claim of polysilafluorene, which is Si−Si coupled in the 1,1 positions.[24] Polymerization via the 1,1 positions is attractive because fluorescence properties of the metallole ring will not be altered significantly and the coiled polymer structures obtained may prevent $\pi$-stacking and self-quenching in thin-film applications. This synthetic approach also requires fewer steps and may provide soluble polymers as a result of the flexible structure. Although Si−Si coupled polymers containing tetraphenylsilole have been prepared,[23] 1,1-silafluorene polymers have not been studied because of the tendency of 1,1-dihydridosilafluorene to yield cyclic structures.[20a,b]

Conjugated organic poly(vinylene)s have been investigated extensively as electron-transporting materials and electroluminescent materials.[25] It would be desirable to prepare metallole−vinylene polymers that incorporate conjugation

(13) Wampler, S. Single-Particle Aerosol Mass Spectrometry. Lawrence Livermore National Laboratory: Livermore, CA; http://www-cmls.llnl.gov/?url=science_and_technology-life_sciences-spams (accessed Nov 27, 2006). Reynolds, J. G. Colorimetric detection for the screening of the presence of High Explosives. Abstracts of Papers, 230th ACS National Meeting, Washington, DC, August 28–September 1, 2005 (2005), ANYL-348.

(14) (a) McQuade, D. T.; Pullen, A. E.; Swager, T. M. *Chem. Rev.* **2000**, *100*, 2537–2574. (b) Toal, S. J.; Trogler, W. C. *J. Mater. Chem.* **2006**, *16*, 2871–2883. (c) Liu, Y.; Mills, R.; Boncella, J.; Schanze, K. *Langmuir* **2001**, *17*, 7452–7455. (d) Chang, C.; Chao, C.; Huang, J. H.; Li, A.; Hsu, C.; Lin, M.; Hsieh, B.; Su, A. *Synth. Met.* **2004**, *144*, 297–301.

(15) (a) Toal, S. J.; Jones, K. A.; Magde, D.; Trogler, W. C. *J. Am. Chem. Soc.* **2005**, *127*, 11661–11665. (b) Toal, S. J.; Magde, D.; Trogler, W. C. *Chem. Commun.* **2005**, *43*, 5465–5467. (c) Sohn, H.; Sailor, M. J.; Douglas, M.; Trogler, W. C. *J. Am. Chem. Soc.* **2003**, *123*, 3821–3830. (d) Sohn, H.; Calhoun, R. M.; Sailor, M. J.; Trogler, W. C. *Angew. Chem., Int. Ed.* **2001**, *40*, 2104–2105.

(16) (a) Geramita, K.; McBee, J.; Shen, Y.; Radu, N.; Tilley, T. D. *Chem. Mater.* **2006**, *18*, 3261–3269. (b) Tang, B. Z.; Zhan, X.; Yu, G.; Lee, P. P. S.; Liu, Y.; Zhu, D. *J. Mater. Chem.* **2001**, *11*, 2974–2978. (c) Sun, Y.; Giebink, N. C.; Kanno, H.; Ma, B.; Thompson, M. E.; Forrest, S. R. *Nature* **2006**, *440*, 908–912. (d) Deng, L.; Furuta, P. T.; Garon, S.; Li, J.; Kavulak, D.; Thompson, M. E.; Frechet, J. M. J. *Chem. Mater.* **2006**, *18*, 386–395. (e) D'Andrade, B. W.; Datta, S.; Forrest, S. R.; Djurovich, P.; Polikarpov, E.; Thompson, M. E. *Org. Electron.* **2005**, *6*, 11–20. (f) Ren, X.; Li, J.; Holmes, R. J.; Djurovich, P. I.; Forrest, S. R.; Thompson, M. E. *Chem. Mater.* **2004**, *16*, 4743–4747.

(17) Tamao, K.; Kawachi, A. *Adv. Organomet. Chem.* **1995**, *38*, 1–58.

(18) (a) Yamaguchi, Y. *Synth. Met.* **1996**, *82*, 149–153. (b) Yamaguchi, S.; Tamao, K. *Bull. Chem. Soc. Jpn.* **1996**, *69*, 2327–2334.

(19) Tamao, K.; Uchida, M.; Izumizawa, T.; Furukawa, K.; Yamaguchi, S. *J. Am. Chem. Soc.* **1996**, *118*, 11974–11975.

(20) (a) Sohn, H.; Huddleston, R. R.; Powell, D. R.; West, R. *J. Am. Chem. Soc.* **1999**, *121*, 2935–2936. (b) Xu, Y.; Fujino, T.; Naito, H.; Dohmaru, T.; Oka, K.; Sohn, H.; West, R. *Jpn. J. Appl. Phys.* **1999**, *38*, 6915–6918. (c) Yamaguchi, S.; Endo, T.; Uchida, M.; Izumizawa, T.; Furukawa, K.; Tamao, K. *Chem. Eur. J.* **2000**, *6*, 1683–1692. (d) Kim, W.; Palilis, L. C.; Uchida, M.; Kafafi, Z. H. *Chem. Mater.* **2004**, *16*, 4681–4686. (e) Lee, S. H.; Jang, B.-B.; Kafafi, Z. H. *J. Am. Chem. Soc.* **2005**, *127*, 9071–9078.

(21) (a) Yamaguchi, S.; Jin, R.-Z.; Tamao, K. *J. Organomet. Chem.* **1998**, *559*, 73–80. (b) Chan, K. L.; McKiernan, M. J.; Towns, C. R.; Holmes, A. B. *J. Am. Chem. Soc.* **2005**, *127*, 7662–7663. (c) Wang, E.; Li, C.; Mo, Y.; Zhang, Y.; Ma, G.; Shi, W.; Peng, J.; Yang, W.; Cao, Y. *J. Mater. Chem.* **2006**, *16*, 4133–4140.

(22) Corriu, R. J. P.; Douglas, W. E.; Yang, Z.-X. *J. Organomet. Chem.* **1993**, *456*, 35–39.

(23) Toal, S. J.; Sohn, H.; Zakarov, L. N.; Kassel, W. S.; Golen, J. A.; Rheingold, A. L.; Trogler, W. C. *Organometallics* **2005**, *24*, 3081–3087.

(24) Chauhan, B. P. S.; Shimizu, T.; Tanaka, M. *Chem. Lett.* **1997**, 785–786.

(25) (a) Burroughs, J. H.; Bradley, D. D. C.; Brown, A. R.; Marks, R. N.; Mackay, K.; Friend, R. H.; Burns, P. L.; Holmes, A. B. *Nature* **1990**, *349*, 539–541. (b) Kim, Y.-H.; Shin, D.-C.; Kwon, S.-K.; Lee, J.-H. *J. Mater. Chem.* **2002**, *12*, 1280–1283. (c) Shim, H.-K.; Jin, J.-I. *Adv. Polym. Sci.* **2002**, *158*, 193–243. (d) Lee, J.-H.; Hwang, D.-H. *Chem. Commun.* **2003**, 2836–2837. (e) Friend, R. H.; Gymer, R. W.; Holmes, A. B.; Burroughes, J. H.; Marks, R. N.; Taliani, C.; Bradley, D. D. C.; dos Santos, D. A.; Bredas, J. L.; Lögdlund, M.; Salaneck, W. R. *Nature* **1999**, *397*, 121–128. (f) Suh, M. C.; Chin, B. D.; Kim. M.-H.; Kang, T. M.; Lee, S. T. *Adv. Mater.* **2003**, *15*, 1254–1258. (g) Friend, R. H.; Burn, P. L.; Holmes, A. B. *Nature* **1990**, *347*, 539–541.

between metallole centers. Hydrosilylation is a technique often used in silane chemistry to form silicon−vinylene functionalities.[26] Addition of the Si−H bond across a carbon−carbon triple bond yields a vinylene product that extends the conjugation and diminishes the band gap in the polymeric material.[27] An attractive feature of polycarbosilanes is the presence of a strong Si−C backbone, as compared to the weaker Si−Si backbone in poly(tetraphenyl)silole.

Reported herein is the synthesis of poly(tetraphenylsilole-vinylene), poly(tetraphenylsilole-silafluorene-vinylene) and poly(silafluorene-vinylene) by catalytic hydrosilylation. This method provides a facile synthetic route to regioregular polymers that retain the inherent electronic properties of the monomers yet incorporate partial delocalization as evidenced by a bathochromic shift in the fluorescence spectra. These polymers include 2,3,4,5-(tetraphenyl)silole and silafluorene moieties directly conjugated through bridging vinylenes by $\sigma^*-\pi/\pi^*$ conjugation. This provides one of the first examples of polymerization of silafluorene in the 1,1 position yielding a UV-blue emitting material. In addition, a new method for the surface detection of TNT, DNT, picric acid (PA), RDX, HMX, Tetryl, TNG, and PETN particulates by an amplified fluorescence quenching pathway is described. Visual detection limits down to the picogram level were achieved. This method allows for efficient sampling of high-priority, low-volatility explosives such as RDX, HMX, and PETN. Ab initio density functional theory (DFT) calculations were used to probe energetic properties of the donor and acceptor on the detection process. In addition, $^{29}$Si NMR spectra provides evidence for Lewis acid–base interactions between basic oxygen atoms of the high explosive molecules and the Si atom of the silacycle chromophore. Poly(silafluorene-vinylene) provides the best energy matching and analyte binding for the explosives studied and proves to be an effective luminescent sensor for nitroaromatics and the nitrate ester−nitramine classes of explosives.

## Results and Discussion

**Model Compounds.** Structural characterization of metallole polymers can be challenging because of peak broadening in the $^1$H NMR spectrum, irregular stereochemistry, and the lack of spectroscopically distinct terminal groups. In an effort to gain insight into the structure and regularity of new metallole-vinylene polymers, we first synthesized model trimeric complexes. As seen in Scheme 1, trimers **1**−**3** were prepared using combinations of various monomers. Yields and analytical purities after several precipitations were good. Elemental analyses of even the highly crystalline materials yielded slightly low carbon analyses, presumably because

**Scheme 1. Synthetic routes to the trimeric model compounds. (a) $H_2PtCl_6$, toluene, 70 °C, 3 h; (b) $H_2PtCl_6$, toluene, 50 °C, 2 h**

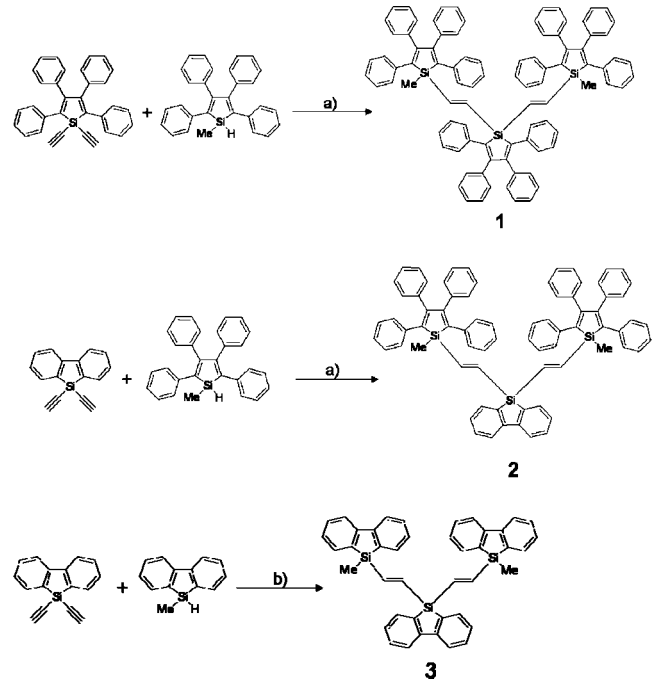


of the formation of silicon carbide in the combustion analysis. This problem was greater in the polymers for which $^{29}$Si NMR spectra (vide infra) also revealed Lewis acidic character, which leads to entrainment of water. $^1$H NMR spectra are included in the Supporting Information to demonstrate purity and entrapped water.

Analysis of the reaction mixture at varying temperatures revealed a high selectivity for hydrosilylation over dehydrocoupling at lower reaction temperatures. The use of thermal control to minimize the dehydrocoupling pathway has been demonstrated previously.[23] Hydrosilylation may also produce both *cis*- and *trans*-products, depending on the steric bulk surrounding the ethynyl functionality. It was important to confirm the stereochemistry in the model compounds, so that the regio-regularity of the key polymerization step was defined. In the case of the silafluorene trimer **3**, $^1$H NMR characterization revealed a *trans*-product. Doublets representing the vinylene hydrogens appear at 7.02 and 6.93 ppm in the $^1$H NMR spectrum. Coupling constants of 22.2 and 22.8 Hz, respectively, are close to the 19 Hz observed for silane substituted *trans*-vinylene products.[28] This result was promising because previous attempts to polymerize secondary silanes by hydrosilylation of simple aryl acetylenes failed to provide regioregular products because of the low steric hindrance around the silicon atom.[29] By placing the ethynyl functionalities directly on the silafluorene, hydrosilylation proceeded exclusively (>98% by NMR) to *trans*-product.

Trimers **1** and **2** were more difficult to characterize by NMR spectroscopy because of overlap between the vinylic hydrogens and the phenyl proton resonances. However, the more sterically hindered tetraphenylsilole should have an

(26) (a) Korshak, V. V.; Sladkov, A. M.; Luneva, L. K. *Izv. Akad. Nauk SSSR, Otd. Khim. Nauk* **1962**, 2251–2253. (b) Luneva, L. K.; Sladkov, A. M.; Korshak, V. V. *Vysokomol. Soedin.* **1965**, *7*, 427–431.
(27) Joo, S.-H.; J., M.-Y.; Ko, D. H.; Park, J.-H.; Kim, K. Y.; Bae, S. J.; Chung, I. J. *J. Appl. Polym. Sci.* **2006**, *100*, 299–306.
(28) Sumiya, K.-I.; Kwak, G.; Sanda, F.; Masuda, T. *J. Polym. Sci., Part A: Polym. Chem.* **2004**, *42*, 2774–2783.
(29) (a) Dong, S. K.; Sang, C. S. *J. Polym. Sci., Part A: Polym. Chem.* **1999**, *37*, 2933–2940. (b) Dong, S. K.; Sang, C. S. *J. Polym. Sci., Part A: Polym. Chem.* **1999**, *37*, 2263–2273.

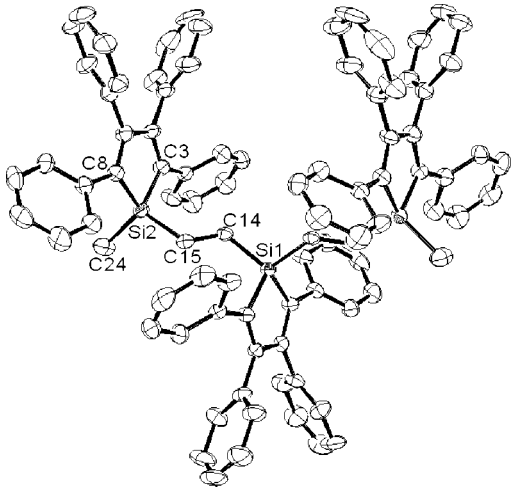


**Figure 2.** Thermal ellipsoid plot of **1** at the 50% probability level. Hydrogen atoms were excluded for clarity. Selected bond lengths (Å): C14−C15 1.309(3). Selected angles (deg): Si2−C15−C14 127.1(2), C15−C14−Si1 124.1(2), C8−Si2−C3 92.55(11), C24−Si2−C15 107.64(12).

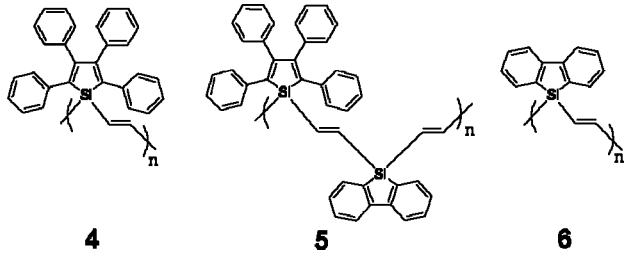


**Figure 3.** Chemical structures of tetraphenylsilole- and silafluorene-vinylene polymers.

even greater preference for the *trans*-product than silafluorene. An attempt to obtain X-ray quality crystals for the trimers proved unsuccessful for the silafluorene containing trimers **2** and **3** but successful for trimer **1**. The structure reveals a *trans*-only product (Figure 2). Yields obtained after recrystallization decreased only slightly, from 73 to 68%, showing that the crystals indeed contain the predominant isomer. The vinylene moiety C14−C15 has a bond length of 1.309(3) Å, which is typical for carbon−carbon double bonds. The torsion angles for Si2−C15−C14 and C15−C14−Si1 are 127.1(2)° and 124.1(2)°, respectively. The former is slightly higher, presumably because of steric interactions between the phenyl substituents of the outer two silole moieties. The internal torsion angle for C8−Si2−C3 is 92.55(11)°, which is close to a typical value of 93.21(6)° observed for silacyclopentadienes.[23] These strained silacycles expose the silicon center to attack by Lewis bases, which will prove to be an important feature for the binding of explosive analytes. Since both 1,1-diethynyl(tetraphenyl) silole (DEsilole) and 1,1-diethynylsilafluorene (DESF) sterically direct *trans*-addition during hydrosilylation, it was concluded that trimer **2** was structurally similar.

**Polymerizations.** With spectroscopic and structural evidence from the model compounds showing that hydrosilylation affords a regioregular *trans*-product in good yield, polymers **4**−**6** were synthesized under similar conditions using 1,1-diethynyl functionalized monomers (Figure 3). Reaction progress was monitored by $^1$H NMR spectroscopy. Polymerization was complete in all cases after 24 h at 70 °C or 48 h at 50 °C. However, increased molecular weights are observed for reactions at 70 °C. The polymers are soluble in common organic solvents, including dichloromethane, toluene, tetrahydrofuran, and ethyl acetate. Low-molecular-weight oligomers, which are present as minor byproducts, may be removed by repeated precipitations from methanol.

**Table 1. Results of Catalytic Hydrosilylation Syntheses of Polymers 4−6**

| polymer | yield (%)[a] | $M_w$ (GPC) | $(M_w/M_n)^b$ | $n$ |
|---|---|---|---|---|
| **4** | 73 | 4000 | 1.15 | 10 |
| **5** | 71 | 4500 | 1.24 | 8 |
| **6** | 66 | 4300 | 1.37 | 21 |
| poly(tetraphenyl)silole | 88 | 1500 | 1.1 | 4 |

[a] Calculated after three precipitations from methanol. [b] Calculated by GPC.

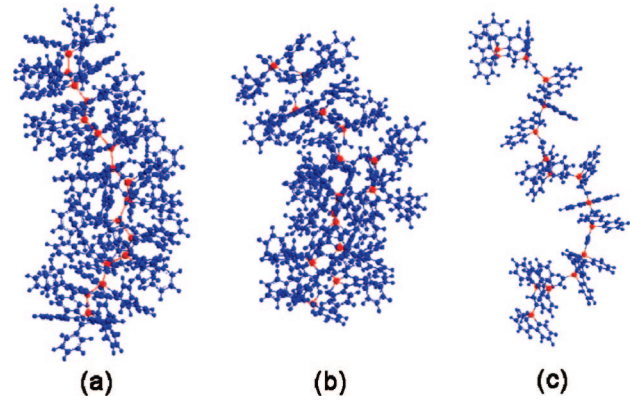


**Figure 4.** Structural comparison of (a) poly(tetraphenyl)silole, $n = 17$; (b) **4**, $n = 15$; (c) **6**, $n = 16$. Red atoms represent the silicon backbone. Polymer structures were simulated using Molecular Mechanics on Chem3D Ultra 9.0.

Molecular weights were determined by GPC (Table 1). The molecular weights of polymers **4**−**6** are slightly higher than those observed for poly(tetraphenyl)silole.[23] They also incorporate a Si−C backbone rather than a Si−Si backbone, whose bonds differ in strength by ∼150 kJ mol$^{-1}$. These polymers are expected to adopt a helical structure similar to that of poly(tetraphenyl)silole (Figure 4). Both polymers **4** and **6** have a more open structure than poly(tetraphenyl)silole. The phenyl substituents around the silacyclopentadiene frame of polymer **4** hinder access to the silicon centers. However, the more porous structure of polymer **6** may allow for effective analyte binding to the Lewis acidic silicon atom.

**Photoluminescence.** Photoluminescence (PL) data were collected on the monomer, trimer, and polymer materials synthesized in this study (Table 2). Polymers **4**−**6** exhibited a ∼13 nm bathochromic shift in $\lambda_{flu}$ from their analogous trimer complexes **1**−**3** along with broadening toward the low-energy side of the emission band (Figure 5). These features suggest an increase in delocalization through the backbone with increasing chain length. Delocalization is more commonly observed in rigid phenylene-type polymers, where bridging alkynyl functionalities allow for a high degree of conjugation between monomer units.[30] However, similar delocalization is seen in poly(tetraphenyl)silole, where a red-shift in fluorescence is a result of $\sigma-\sigma^*$ conjugation of the Si-Si backbone.[23] In the present case, the vinylene bridge

**Table 2. Summary of Photoluminescence Data for Monomers, Trimers, and Polymers**

| metallole | $\lambda_{abs}$ (nm)[a] | $\epsilon_{max}$ (L mol$^{-1}$cm$^{-1}$)[b] | solution $\lambda_{flu}$ (nm)[a] | thin-film $\lambda_{flu}$ (nm)[c] | $\Phi_{flu}$[d] (%) |
|---|---|---|---|---|---|
| DEsilole | 305, 390 | 7500 | 490 | 485 | 0.13 |
| DESF | 291, 324 | 7700 | 356 | 365 | 24 |
| 1 | 304, 388 | 18000[e] | 480 | 487 | 0.40 |
| 2 | 296, 381 | 9400[e] | 478 | 483 | 0.30 |
| 3 | 290 | 20400[e] | 349 | 357 | 6.1 |
| 4 | 304, 389 | 2900 | 493 | 490 | 1.0 |
| 5 | 297, 390 | 1800 | 492 | 486 | 2.0 |
| 6 | 294 | 6300 | 362 | 376 | 4.3 |

[a] UV–vis and fluorescence taken in toluene. [b] Absorptivities are calculated per mole of metalloid. [c] Emission maximum for thin layer of fluorophore absorbed onto TLC plate. [d] Quantum yield of fluorescence ± 30%, relative to 9,10-diphenylanthracene[31] in toluene. [e] Absorptivities per metallole are one-third of the reported value.

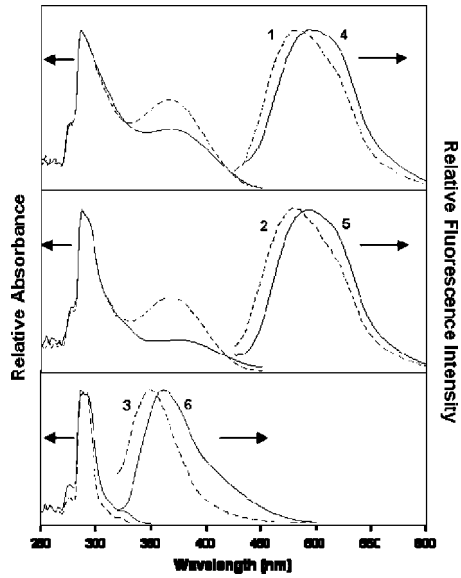


**Figure 5.** UV–vis and fluorescence spectra of model trimers **1**−**3** (dotted lines) as compared with polymers **4**−**6** (solid lines) showing a bathochromic emission shift for the polymers.

of polymers **4**−**6** allows partial $\sigma^*$(Si−C)−$\pi$(vinylene) conjugation along the backbone in the ground state and $\sigma^*$(Si−C)−$\pi^*$(vinylene) conjugation in the lowest excited state (Figure 6). The crystal structure of **1** reveals a rms out-of-plane angle between the two vinylene bridges of 76.7°. This orientation, with respect to the face of the silole ring, is such that the $\pi$-orbitals involved in the carbon−carbon double bond are directed toward the $\sigma^*$ and $\pi^*$ orbitals of the silole ring. Orbital overlap thereby allows for delocalization throughout the polymer via the bridging vinylene. This is supported by density functional theory (DFT) calculations presented later. Polymer **5** shows an emission band at 492 nm, which is similar to that of polymer **4** and characteristic of tetraphenylsilole emission. The lack of emission from the silafluorene moiety of polymer **5** also suggests the presence of electronic communication through the polymer chain. It is typical for tetraphenylsiloles, which

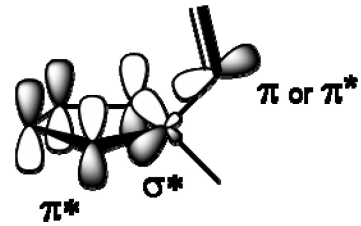


**Figure 6.** Depiction of the orbital overlap between the vinylene bridge and LUMO of the silacylcopentadiene ring. Structural orientation is based on the crystal structure data of trimer **1**. Phenyl rings and hydrogens are omitted for clarity. The $\pi^*$(butadiene)−$\sigma^*$(Si) orbital overlap forms the LUMO of the silole moiety. The $\pi$ orbital of the vinylene bridge overlaps with the silole LUMO, accounting for the ground-state orientation in **1**. In the excited state, overlap of the $\pi^*$ vinylene orbital with the silole LUMO is observed in the DFT calculations (see the Supporting Information, LUMO figure e) and accounts for red shifting of the emission spectra in metallole polymers **4**-**6**.

have a lower LUMO than silafluorenes, to act as sinks for excitons in delocalized copolymer systems.[31]

Solid-state PL data was collected to determine the effect of aggregation during thin-film explosives detection studies. Two different techniques were used. The first method involved spin-casting toluene solutions of the materials onto quartz discs.[32] This technique has been widely used for solid-state fluorescence characterization of functional polymeric materials. Quartz provides a smooth, UV-transparent surface, and the emission spectrum of the film reflects polymer stacking effects. However, this method requires a high solubility of the polymer in appropriate volatility solvents, high molecular weights for casting uniform films, large amounts of sample, and is expensive and time-consuming.[33] The second method employs absorption of the polymer dissolved in $CHCl_3$ (4.0 mg mL$^{-1}$) spotted onto the silica gel of a thin-layer chromatography (TLC) plate. This technique was used by Tang et al. to more conveniently analyze the solid-state PL properties of various tetraphenylsiloles with good reproducability.[34] The silica surface is porous and adsorption may alter the packing properties of more rigid polymers, such as **7**. Both methods were studied to gain insight into the solid-state spectral properties. Figure 7 compares these different approaches with the solution-phase fluorescence spectra of polymers **4** and **6**. Polymer **4** shows no significant change in $\lambda_{flu}$ for each substrate used. This suggests that there is minimal interchain electronic communication in the solid-state and that the TLC method is a useful and spectroscopically reliable method for measuring the solid-state PL properties of tetraphenylsilole polymers. However, the emission spectrum of polymer **6** shows an increasing bathochromic shift from solution to TLC to quartz substrates. This suggests that the packing of the more rigid silafluorene framework becomes more ordered in the

(30) (a) Geisa, R.; Schulz, R. C. *Makromol. Chem.* **1990**, *191*, 857–867. (b) Lampert, R. A.; Meech, S. R.; Metcalf, J.; Phillips, D.; Schapp, A. P. *Chem. Phys. Lett.* **1983**, 137–140. (c) Maulding, D. R.; Roberts, B. G. *J. Org. Chem.* **1969**, *34*, 1734–1736. (d) Grem, G.; Leditzky, G.; Ullrich, B.; Leising, G. *Adv. Mater.* **1992**, *1*, 36–37. (e) Swager, T. M.; Gil, C. J.; Wrighton, M. S. *J. Phys. Chem.* **1995**, *99*, 4886–4893.

(31) Habrard, F.; Ouisse, T.; Stéphan, O.; Aubouy, L.; Gerbier, Ph.; Hirsch, L.; Huby, N.; Van der Lee, A. *Synth. Met.* **2006**, *156*, 1262–1270.

(32) Solutions (30 mg/mL) of **1**−**6** were spin-cast from toluene for 1 min at 2000 rpm. The 25 mm × 25 mm quartz substrate plates were cleaned by sonication in acetone and methanol for 10 min each. Dichloromethane was then spin-cast onto the quartz plate to remove any residual particulate contamination.

(33) Kraft, A.; Grimsdale, A. C.; Holmes, A. B. *Angew. Chem., Int. Ed.* **1998**, *37*, 403–428.

(34) Chen, J.; Law, C. C. W.; Lam, J. W. Y.; Dong, Y.; Lo, S. M. F.; Williams, I. D.; Zhu, D.; Tang, B. Z. *Chem. Mater.* **2003**, *15*, 1535–1546.

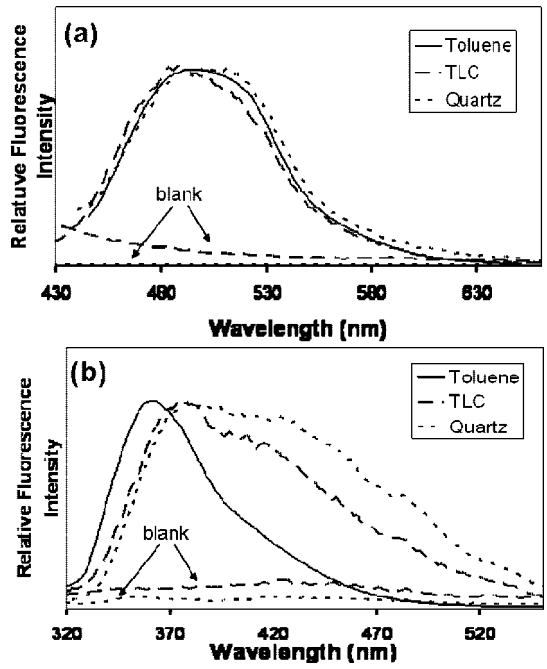


**Figure 7.** Solid-state photoluminescence data for polymers (a) **4** and (b) **5** collected on silica TLC plates and quartz discs. Data for a blank TLC plate and a blank quartz disk are shown.

solid state. This is likely the result of interchain $\pi-\pi$ stacking interactions that lead to red-shifted excimer emission. Although not unexpected, this trend will need to be taken into consideration when choosing substrates for explosives detection applications.

Solution-phase quantum yields of fluorescence ($\Phi_{flu}$) increased for polymers **4** and **5** from their analogous trimer complexes **1** and **2** (Table 2). This supports the hypothesis that the polymers adopt more rigid, coiled structures. The trimers and polymers synthesized from the tetraphenylsilole monomer exhibit an increased $\Phi_{flu}$ through steric crowding, which is expected to hinder phenyl ring rotation. This phenomenon has been extensively documented by the observed aggregated induced emission (AIE) of precipitated silole nanoparticles.[35] The emission quantum efficiency of polymer **6** decreased slightly from trimer **3**. Even with a slight decrease in $\Phi_{flu}$, **3** and **6** exhibit quantum efficiencies several orders of magnitude higher than tetraphenylsilole counterparts in the solution phase. This may be attributed to the structural rigidity of the silafluorene moiety, which reduces the number of nonradiative decay pathways. The addition of the vinylene bridges into the polymer may also contribute to the good quantum yields of fluorescence.[36] The lack of reliable reference materials prevents the calculation of absolute solid-state quantum yields for most polymeric materials.[37] When compared to poly(tetraphenyl)silole, polymers **4**−**6** also exhibit an overall increase in the relative solid state fluorescence quantum efficiencies. This, along with exciton delocalization along the polymer backbone, is an important characteristic for fluorescence sensing applications. More efficient luminescence effectively reduces background interferences during detection. It also requires less material to be used, decreasing the overall cost of the detection. Delocalization of excitons throughout a conjugated polymer improves sensing by amplified fluorescence quenching of entire polymer chains by a single analyte molecule.[14a]

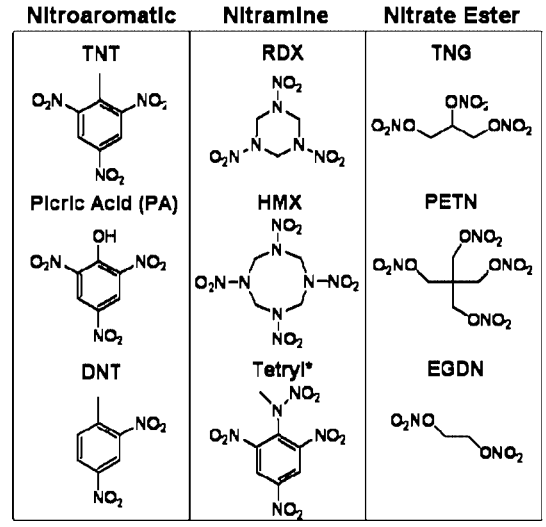


**Figure 8.** Structures of common high explosives categorized by functional group class.

**Explosives Detection by Fluorescence Quenching.** The widely used high explosives contain nitroaromatic, nitrate ester, and nitramine functionalities (Figure 8). Detection of these explosives requires targeting a specific chemical or physical property. Detection by amplified fluorescence quenching presumably involves electron transfer from the polymer fluorophore to the lowest unoccupied molecular orbital (LUMO) of the explosive materials. In this study, solution-phase Stern−Volmer quenching studies were initially carried out for **4**−**6** in toluene solvent to characterize the fluorescence quenching efficiency of several common explosive materials (2,4,6-trinitrotoluene (TNT), picric acid (PA), 2,6-dinitrotoluene (DNT), and cyclotrimethylenetrinitramine (RDX)). The Stern−Volmer constant is calculated using eq 1.

$$(I_0/I) - 1 = K_{sv}[A] \quad (1)$$

Polymers **4**−**6** exhibit linear Stern−Volmer plots for the explosives studied at concentrations below $3.0 \times 10^{-4}$ M. The Stern−Volmer constants are summarized in Table 3. These constants are a quantitative measure of explosives detection efficiency. Data for poly(tetraphenyl)silole is

(35) (a) Yin, S.; Peng, Q.; Shuai, Z.; Fang, W.; Wang, Y.-H.; Luo, Y. *Phys. Rev. B: Condens. Matter* **2006**, *73*, 205409/1–205409/5. (b) Bhongale, C. J.; Chang, C.-W.; Diau, E. W.-G.; Hsu, C.-S.; Dong, Y.; Tang, B.-Z. *Chem. Phys. Lett.* **2006**, *419*, 444–449. (c) Chen, J.; Xu, B.; Yang, K.; Cao, Y.; Sung, H. H. Y.; Williams, I. D.; Tang, B. Z. *J. Phys. Chem. B* **2005**, *109*, 17086–17093. (d) Ren, Y.; Lam, J. W. Y.; Dong, Y.; Tang, B. Z.; Wong, K. S. *J. Phys. Chem. B* **2005**, *109*, 1135–1140.

(36) (a) Wolak, M. A.; Delcamp, J.; Landis, C. A.; Lane, P. A.; Anthony, J.; Kafafi, Z. *Adv. Funct. Mater.* **2006**, *16*, 1943–1949. (b) Wolak, M. A.; Melinger, J. S.; Lane, P. A.; Palilis, L. C.; Landis, C. A.; Anthony, J. E.; Kafafi, Z. H. *J. Phys. Chem. B* **2006**, *110*, 10606–10611. (c) Wolak, M. A.; Melinger, J. S.; Lane, P. A.; Palilis, L. C.; Landis, C. A.; Delcamp, J.; Anthony, J. E.; Kafafi, Z. H. *J. Phys. Chem. B* **2006**, *110*, 7928–7937. (d) Jang, B.-B.; Lee, S. H.; Kafafi, Z. H. *Chem. Mater.* **2006**, *18*, 449–457.

(37) Yang, J.-S.; Swager, T. M. *J. Am. Chem. Soc.* **1998**, *120*, 5321–5322.

**Table 3. Summary of Stern−Volmer Constants ($K_{sv}$) for Polymer Fluorescence Quenching with Explosive Analytes Reported in $M^{-1}$ in Toluene Solution; Detection of RDX Was Not Observed for Polymers 4−6**

| polymers | TNT | DNT | PA |
|---|---|---|---|
| 4 | 10500 | 4300 | 16400 |
| 5 | 9900 | 4100 | 15600 |
| 6 | 10200 | 5500 | 20100 |
| poly(tetraphenyl)silole[a] | 4300 | 2400 | 11000 |

[a] See ref 22.

included in the table for comparison. Polymers **4**−**6** show a higher quenching efficiency than obtained with poly(tetraphenyl)silole. This may be due to enhanced amplified quenching expected for the higher-molecular-weight polymers. In addition, improved conjugation throughout the backbone of the polymer may increase the quenching. RDX was not detectable in solution within the noise limits of the fluorimeter.

The high Stern−Volmer quenching constants observed for the detection of nitroaromatic explosives prompted us to investigate solution polymer−analyte interactions using $^{29}$Si NMR. Strained silacycles have found use as effective Lewis acid catalysts.[38] The rigid nature of the metallocyclopentadiene unit and the small internal C−Si−C angle of these systems (∼90°) make them candidate Lewis acids. Even though $\pi-\pi$ interactions may facilitate association of some aromatic explosives with the polymer, the nitro or nitrate substituents found in most high explosives may act as Lewis bases, forming an acid–base adduct with the acidic silicon centers in these systems. Because of the broad and weak $^{29}$Si NMR signal observed for the polymers, trimer **3** was used to model these interactions (Figure 9). Two resonances corresponding to the outer silicon centers and the central silicon center are observed in the $^{29}$Si NMR spectrum. An internal tetramethylsilane (TMS) reference, separated from the sample matrix using a tapered glass insert, was used. This reference was set to 0 ppm in all cases. Upon exposure to TNT, both polymer $^{29}$Si peaks shifted downfield relative to the external TMS reference. The central silicon center of the trimer shifts more (0.125 ppm) than the outer silicon centers (0.101 ppm), suggesting a better interaction with TNT analyte. This implies that nitro-containing high explosives may bind weakly to the silicon centers of these polymers, which would orient them for efficient inner sphere electron transfer with the excited-state of the polymer. This helps explain why silole and silafluorene containing polymers are generally excellent explosive sensors. These Lewis acid–base interactions also explain the unusual tendency of these hydrophobic polymers to readily absorb about one equivalent of water per Si, which is often observed in the elemental analysis of the solid tetraphenylsilole and silafluorene polymers, as well as by $^1$H NMR spectroscopy after dissolution.

The electrostatic potential (Mullikan charges) modeled by ab initio DFT calculations for trimer **3** shows a positive

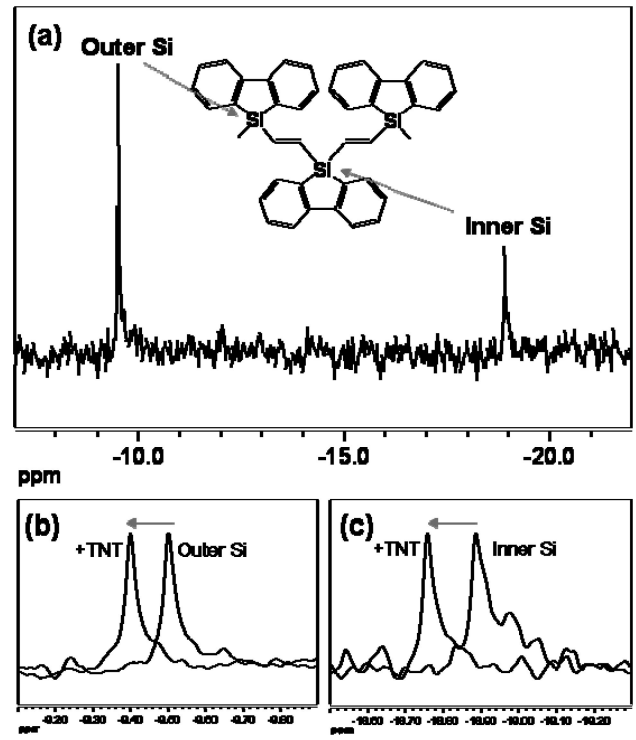


**Figure 9.** $^{29}$Si NMR spectra of trimer **3**. Spectra taken in $d_6$-benzene at a concentration of 100 $mL^{-1}$. TMS was used as an internal capilliary standard referenced to 0 ppm. (a) Both peaks corresponding to the different silicon environments. (b) A downfield shift of the outer Si peak upon exposure to 12 equiv of TNT. (b) A downfield shift of the inner Si peak on exposure to 12 equiv of TNT.

charge distribution centered on the silicon atoms (Figure 10). The $^1$SOMO was calculated to model the excited-state orbital from which the electron is transferred from the polymer sensor to the analyte. A static quenching model, which implies preassociaton of the explosive analyte, has been established through previous fluorescence quenching lifetime studies.[15c] Figure 10 depicts the molecular orbital density of the LUMO for trimer **3** and the LUMO for TNT. The LUMO of **3** resides primarily on or near the central silicon. The LUMO for TNT is localized on the aromatic system and the nitro oxygen atoms. Thus, a ground-state Lewis acid–base interaction between nitro groups of TNT and the silicon centers of trimer **3** facilitates orbital overlap between the two and provides an efficient inner-sphere pathway for electron-transfer quenching of the excited state. Even though trimer **3** effectively binds the explosive analytes and can be used as an explosives sensor, the advantage of using polymers is 2-fold. Delocalization in conjugated polymers allows for amplified detection at any point along the polymer chain.[39] Also, extended conjugation red shifts the emission toward visible solid-state luminescence in polymer **6**. This is important in thin-film imaging applications by visible fluorescence.

Given the limited practical applicability of solution-phase explosives detection, we explored a surface sensing method for imaging trace explosives particulates using thin films of polymers **4**−**6**. A detailed procedure for this method can be found in the experimental section. Detection limits for this method are reported in nanograms per square centimeter to emphasize the quantity of explosive deposited in the given

(38) (a) Shirakawa, S.; Lombardi, P. J.; Leighton, J. L. *J. Am. Chem. Soc.* **2005**, *127*, 9974–9975. (b) Kinnaird, J. W. A.; Ng, P. Y.; Kubota, K.; Wang, X.; Leighton, J. L. *J. Am. Chem. Soc.* **2002**, *124*, 7920–7921.
(39) (a) Zhou, Q.; Swager, T. M. *J. Am. Chem. Soc.* **1995**, *117*, 12593–12602. (b) Zhou, Q.; Swager, T. M. *J. Am. Chem. Soc.* **1995**, *117*, 7017–7018.

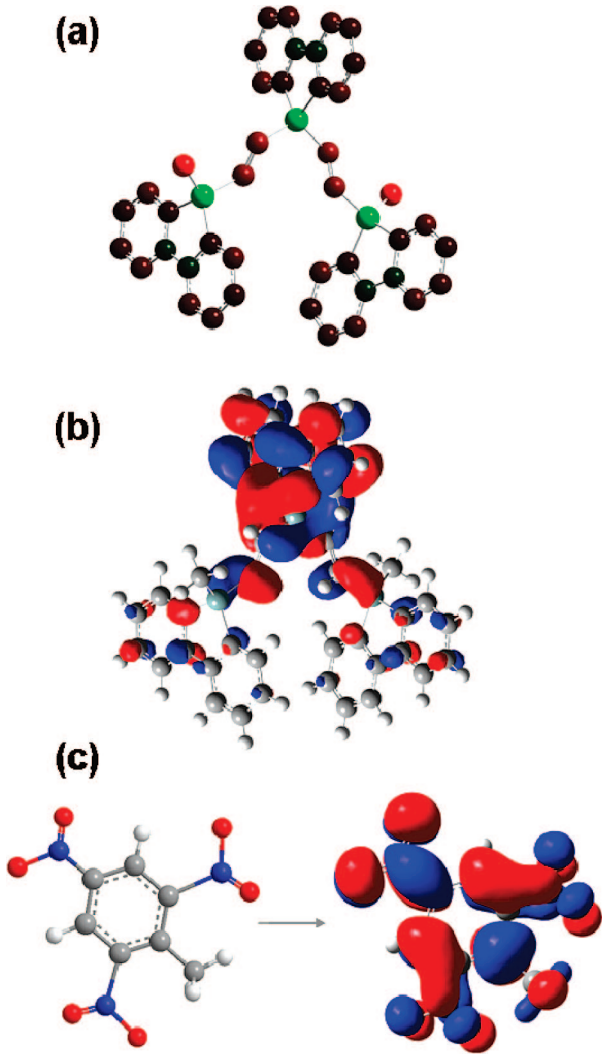


**Figure 10.** Ab initio DFT calculations on trimer **3** and TNT at the B3LYP/6–31G* level. (a) Electrostatic potentials for **1**. Colors range from –0.668 to +0.668, with green denoting the electron-deficient regions and red denoting the electron-rich regions. (b) Lowest unoccupied molecular orbital (LUMO) of **3**. (c) LUMO of TNT.

area. The explosives studied by this detection method were expanded to include cyclotetramethylene-tetranitramine (HMX), 2,4,6-trinitrophenyl-N-methylnitramine (Tetryl), trinitroglycerin (TNG), and pentaerythritol tetranitrate (PETN). Dinitroethylene glycol (EGDN) and the explosives taggant 2,3-dimethyl-2,3-dinitrobutane (DMNB) are too volatile ($P_{vap}$ = 2.8 × $10^{-2}$ and 2.1 × $10^{-3}$ Torr, respectively) to be detected at a 64 ng cm$^{-2}$ limit using this surface detection method due to their rapid evaporation.

As expected, polymer **4** undergoes quenching only by nitroaromatic explosives. However, copolymer **5** is able to detect both RDX and nitroaromatic explosives when illuminated at 254 nm, but not upon illumination at 360 nm. Polymer **6** detects the entire range of explosives at much lower detection limits than either polymer **4** or **5**. A photograph of the solid-state detection of RDX using polymer **6** is seen in Figure 11. Even though RDX is unable to effectively quench the luminescence of polymer **6** in solution, it very efficiently quenches the polymer luminescence in the solid state with a detection limit of 2 ng cm$^{-2}$. This suggests that the close proximity of polymer and analyte in solid-

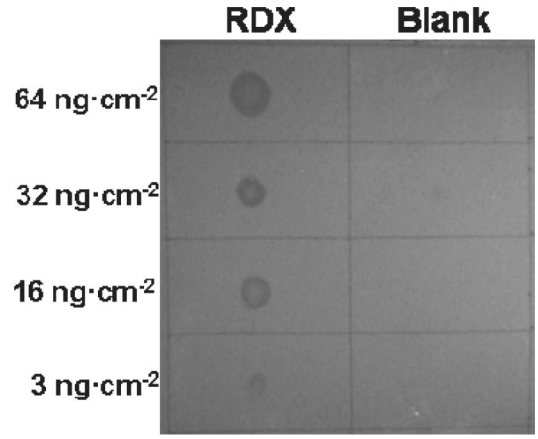


**Figure 11.** Fluorescence quenching of polymer **6** by solid particulates of RDX in a thin film on filter paper as observed using a Sony 2.0 megapixel digital camera as a black and white image (right) under continuous UV irradiation (254 nm).

state detection studies facilitates the excited-state electron transfer process, resulting in improved detection of non-nitroaromatic explosives. Weak Lewis acid–base interactions may help orient the explosive-metallole moieties for efficient excited-state electron transfer in the solid-solution film studies, but would be much less important in quenching experiments performed in very dilute solutions. The detection of a large range of trace explosive particles by UV-blue-emitting polymer **6** reveals that effective energy matching through frontier molecular orbital tuning is another factor to consider when designing polymeric sensors.[40] Typically, nonconjugated explosive materials, which make up the majority of nitrate ester- and nitramine-based explosives, have more negative reduction potentials than conjugated aromatic explosive materials, rendering them difficult to detect by fluorescence quenching. Polymer **6** exhibits a wider band gap, as seen by its UV-blue emission band, as compared to polymers **4** and **5**. This produces a better redox driving force with a wider range of explosives.

To see whether the electron accepting ability of the explosive analyte correlated with ease of detection, theoretical calculations at the B3LYP/6–31G* level of theory were used to determine the HOMO and LUMO energies for the optimized structures of the explosive analytes. The frontier molecular orbital energies as well as the $^1$SOMO of trimers **1** and **3** were also calculated to model the energies of the polymer donors **4** and **6**. The calculated band gap energies of the explosives were found to agree well with the first absorptions observed in the UV–vis spectra and the calculated LUMO energies correlate well with measured redox potentials for TNT, RDX, and HMX.[41] Delocalization within the trimers was observed in the calculations by comparing band gap energies with previous calculations on the mono-

(40) Thomas III, S. W.; Amara, J. P.; Bjork, R. E.; Swager, T. M. *Chem. Commun.* **2005**, 4572–4574.
(41) (a) Saravanan, N. P.; Venugopalan, S.; Senthilkumar, N.; Santhosh, P.; Kavita, B.; Prabu, H. G. *Talanta* **2006**, *69*, 656–662. (b) Orloff, M. K.; Mullen, P. A.; Rauch, F. C. *J. Phys. Chem.* **1970**, *74*, 2189–2192. (c) Chaloosi, M.; Gholamian, F.; Zarei, M. A. *Propellants, Explosives, Pyrotechnics* **2001**, *26*, 21–25.

**Table 4. Solid-State Detection Limits (ng cm$^{-2}$) for Trace Explosives by Fluorescence Quenching of Sprayed-On Films of Polymers 4−6[a]**

| | | 4 | | 5 | | 6 | |
|---|---|---|---|---|---|---|---|
| explosive | $P_{vap}$ (Torr) at 25 °C | porcelain | filter paper | porcelain | filter paper | porcelain | filter paper |
| Tetryl | $5.7 \times 10^{-9}$ | 0.3 | 1 | 1 | 1 | 2 | 0.2 |
| TNT | $5.8 \times 10^{-6}$ | 0.6 | 2 | 0.6 | 0.6 | 2 | 0.3 |
| PA | $5.8 \times 10^{-9}$ | 2 | 2 | 16 | 2 | 3 | 2 |
| RDX | $4.6 \times 10^{-9}$ | | | | 32 | 16 | 2 |
| PETN | $1.4 \times 10^{-8}$ | | | | | 16 | 2 |
| DNT | $1.1 \times 10^{-4}$ | 32 | 3 | 2 | 3 | 16 | 2 |
| HMX | $8.0 \times 10^{-11}$ | | | | | 32 | 3 |
| TNG | $4.4 \times 10^{-4}$ | | | | | | 3 |

[a] A blank value represents no detection at the 64 ng cm$^{-2}$ level.

**Table 5. HOMO and LUMO Energies Calculated for the Various Explosives and Trimers 1 and 3 at the B3LYP/6–31G* Level of Theory[a]**

| compd | LUMO (eV) | HOMO (eV) | band gap (eV) |
|---|---|---|---|
| octanitrocubane | −4.463 | −9.823 | 5.361 |
| tetryl | −3.918 | −8.109 | 4.109 |
| picric acid | −3.891 | −8.218 | 4.327 |
| TNT | −3.483 | −8.435 | 4.952 |
| PETN | −3.075 | −8.707 | 5.633 |
| CL-20 | −3.020 | −8.816 | 5.796 |
| DNT | −2.966 | −8.109 | 5.143 |
| HMX | −2.721 | −8.299 | 5.578 |
| RDX | −2.531 | −8.245 | 5.714 |
| TNG | −2.476 | −9.088 | 6.612 |
| EGDN | −2.122 | −8.898 | 6.775 |
| DMNB | −2.068 | −8.027 | 5.959 |
| TATP | 0.354 | −6.340 | 6.694 |
| HMTD | 0.680 | −6.313 | 6.993 |
| **1** | −1.741 (−2.159) | −5.252 | 3.511 (3.093) |
| **3** | −1.116 (−1.942) | −5.769 | 4.653 (3.827) |

[a] Values in parentheses are the calculated $^1$SOMO energies and corresponding band-gaps.

mer.[42] For example, the band gap for trimer **3** is 4.65 eV, whereas the band gap for the silafluorene monomer is 4.97 eV. The $^1$SOMO energies of the polymers should be slightly lower in energy (0.1 eV) than those calculated for the trimers because of further delocalization, as observed in the red-shifted UV–vis and fluorescence spectra. Table 5 lists the results for the calculated HOMO and LUMO energies for each explosive studied, as well as the $^1$SOMO of **1** and **3**. The explosives are tabulated in descending order of LUMO energies. These energy levels are expected to represent the relative ease of transferring an electron to each explosive in the fluorescence quenching process.

The excited-state energies of **1** and **3** were plotted on the same scale as the molecular orbital calculations for the explosives (Figure 12). The $^1$SOMO energies for the trimers lie within the range of LUMO energies of the explosive analytes detected. Trimer **3** is at a higher energy and thus maintains a better driving force for electron transfer to the explosives than trimer **1**. The trend observed in the detection limits for all the explosives parallels the LUMO energy of each explosive in remarkably good agreement. This good correlation between theoretical and experimental results

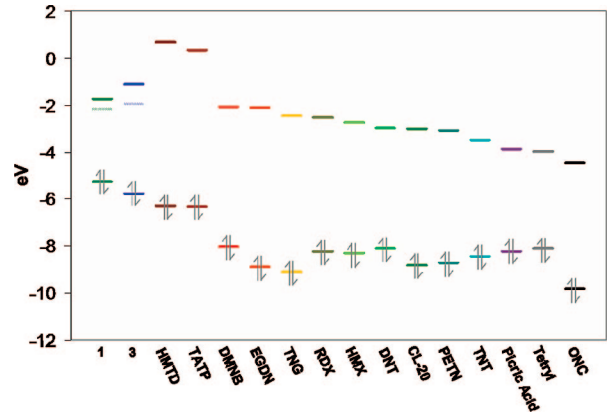


**Figure 12.** Frontier orbital energy correlation diagram for model trimers **1** and **3** with various explosive analytes. Models **1** and **3**: bottom lines represent the HOMO energies; top lines represent the LUMO energies; the middle lines (broken) represent the singlet excited-state energies ($^1$SOMO) calculated with spin polarization. This is the orbital energy from which the excited-state electron transfer process takes place. Explosives: bottom lines represent the HOMO energies; top lines represent the LUMO energies.

supports the conclusion that the LUMO energy of explosive analytes is an important factor in the fluorescence quenching process.

The highly delocalized nitroaromatic explosives generally have lower LUMO energies and are detected much better by fluorescence quenching sensors than aliphatic nitro- and nitrate-based explosives. PETN is an exception to the perfect correlation with LUMO energies. It has LUMO a energy comparable to DNT, HMX, and RDX. Using the calculated LUMO energy for PETN, it would be expected that both tetraphenylsilole and silafluorene polymers would be able to detect this explosive. In practice, only polymer **6** is able to detect PETN at nanogram levels. This result suggests that although frontier orbital energy matching is a dominant factor, it is not the only variable that determines explosives detection in the solid state. The high volatility of EGDN and DMNB prevented their detection even though their calculated LUMO energies lie slightly below those calculated for the trimers. Other high-priority explosives such as triacetone triperoxide (TATP), hexamethylene triperoxide diamine (HMTD), 2,4,6,8,10,12-hexanitro-2,4,6,8,10,12-hexaaza-isowurtzitane (CL-20),[43] and octanitrocubane (ONC)[44] were calculated and are included in the plot of Figure 11. The difficulty in obtaining analytical samples and shock sensitivity of these explosives prevented direct analysis. However, the calculations strongly suggest that the LUMO energies for peroxide-based explosives are far too high to act as effective electron acceptors for a photoinduced electron-transfer process using typical fluorescent polymers. However, the LUMO energies for CL-20 and ONC fall well within the range of detectable explosives using polymers **4–6**. It

(42) Kawabata, H.; Ishida, K.; Matsushige, K.; Tachikawa, H. *Proceedings of the International Symposuim on Super-Functionality of Organic Devices*, Chiba University, Chiba, Japan, Oct 25−28, 2004; IPAP Conference Series 6; Institute of Pure and Applied Physics: Tokyo, 2005; pp 4245

(43) (a) Nielsen, A. T.; Chafin, A. P.; Christian, S. L.; Moore, D. W.; Nadler, M. P.; Nissan, R. A.; Vanderah, D. J.; Gilardi, R. D.; George, C. F.; Flippen-Anderson, J. L. *Tetrahedron* **1998**, *54*, 11793–11812. (b) Simpson, R. L.; Urtiew, P. A.; Ornellas, D. L.; Moody, G. L.; Scribner, K. J.; Hoffman, D. M. *Propellants, Explos., Pyrotechn.* **1997**, *22*, 249–255.

(44) (a) Zhang, M.-X.; Eaton, P. E.; Gilardi, R. *Angew. Chem., Int. Ed.* **2000**, *39*, 401–404. (b) Eaton, P. E.; Zhang, M.-X.; Gilardi, R.; Gelber, N.; Iyer, S.; Surapaneni, R. *Propellants, Explos., Pyrotech.* **2002**, *27*, 1–6.

would be predicted that CL-20 would be detected at limit range of about 1–5 ng $cm^{-2}$. The highly sensitive ONC explosive has the lowest calculated LUMO energy and therefore is predicted to be the easiest explosive for detection, purely on the basis of energetic considerations.

Selectivity and insensitivity to common interferents are other important considerations when developing an explosive sensing polymer. Polymers **4**−**6** as well as poly(tetraphenyl)silole show no change in luminescence when exposed to common organic solvents such as THF, toluene, and methanol. Benzophenone and benzoquinone are typically analyzed for their effectiveness as redox interferents in the detection of explosives by fluorescence quenching. Pentiptycene-derived polymers show some sensitivity toward these interferents.[37] Polymers **4** and **5**, as well as poly(tetraphenyl)silole, show no response to benzophenone. However, polymer **6** is quenched by benzophenone particulates down to 3 ng $cm^{-2}$. This further supports the hypothesis that both reduction potentials and electronic overlap play an important role in the thin-film fluorescence quenching mechanism. Polymer **6** has a wider band gap than the tetraphenylsilole-containing polymers, thus increasing its ability to detect a wider range of electron-accepting materials. Also, the lone pairs that reside on the carbonyls of benzophenone and benzoquinone may effectively bind as Lewis bases to the strained silacycle containing polymer. Future studies will focus on improving molecular recognition aspects so as to increase selectivity and sensitivity toward specific classes of explosives.

## Conclusions

New metallole-vinylene polymers **4**−**6** have been synthesized for use as fluorescent chemosensors for the detection of high explosives. Crystal structure analysis of model trimer complexes and fluorescence emission comparisons between polymers and trimers show a regioregular *trans*-product conjugated through the silicon vinylene bonds. The high quantum efficiencies (especially for polymer **6**), partial conjugation through the backbone, and multiple analyte binding mechanisms yield high Stern−Volmer quenching constants for nitroaromatic explosives such as TNT, DNT, and PA in solution. The open structure of polymer **6** as compared to polymers **4** and **5** allows for Lewis acid–base interactions of analytes with the silacycle ring. The high-energy band gap of **6** allows for the detection of a wider range of explosive materials, including the important high explosives RDX, HMX, TNG, and PETN in the solid state. Theoretical calculations show that LUMO energies of explosives closely follow the observed detection limits obtained with these silicon containing polymers. By tuning the band gap of the fluorescence sensors, relative detection sensitivities can be predicted on the basis of matching the excited-state energies with the LUMO energies of the explosives. Solid-state detection of explosive particulates using silafluorene-containing polymer **6** provides very low detection limits by a rapid, simple sensing method. Optimizing the energy match and thereby lowering the activation energy barrier for the electron-transfer process between the explosive analytes and the sensing polymer appears to be a crucial factor. Polymers **4**−**6** also show promise as a new generation of conjugated and stable organometallic polymers for blue-emitting optical electronic materials.

## Experimental Section

**General.** *Caution: TNT and picric acid are high explosives and should be handled only in small quantities. Picric acid also forms shock-sensitive compounds with heavy metals. Purchased explosive standards were handled as dilute solutions to eliminate an explosion hazard.* All synthetic manipulations were carried out under an atmosphere of dry argon gas using standard Schlenk techniques. Dry solvents were purchased from Aldrich Chemical Co. Inc. and used after purification with an MBraun Auto Solvent Purification System. Spectroscopic-grade toluene from Fisher Scientific was used for the fluorescence measurements. Monomers, 1,1-dihydrido(tetraphenyl)silole, 1,1-dihydridosilafluorene, 2,2′-dibromobiphenyl, 1,1-diethynyl-(tetraphenyl)silole, 1-methyl-1-hydrido(tetraphenyl)silole, 1-methyl-1-hydridosilafluorene, and 1,1-dichlorosilafluorene were synthesized by literature procedures.[24,45–49] All other reagents were purchased from Aldrich Chemical Co. and used as received. Picric acid and DNT were purchased from Aldrich Chemical Co. and recrystallized from ethanol and methanol, respectively. TNT was prepared from DNT[50] and recrystallized from toluene. RDX, HMX, Tetryl, TNG, and PETN were purchased as 1 mg/mL analytical standards in acetonitrile from Cerilliant.

NMR data were collected with the use of a Varian Unity 300 or 500 MHz spectrometer (300.1 MHz for $^{1}H$, 77.5 MHz for $^{13}C$, and 99.4 MHz for $^{29}Si$ NMR). Infrared spectra were obtained with the use of a Nicolet Magna-IR Spectrometer 550. GPC-RI data were obtained with the use of a Viscotek GPCmax VE 2001 GPC and a Viscotek VE 3580 refractive index detector calibrated with polystyrene standards. Fluorescence emission and excitation spectra were recorded with the use of a Perkin-Elmer luminescence spectrometer LS 50B. UV–vis spectra were obtained with the use of a Hewlett-Packard 8452A diode array spectrometer.

**X-ray Crystal Structure Determination.** Diffraction intensity data were collected with a Bruker P4/CCD Smart Apex CCD diffractometer at 100 K. Compound **1** diffracted very weakly, limiting data to about 1.0 Å resolution. The correctness of the centrosymmetric assignment was based on the clear presence of 2-fold rotational symmetry. The structure was solved by direct methods, completed by subsequent difference Fourier syntheses, and refined by full matrix least-squares procedures on $F^2$. SADABS absorption corrections were applied to all data. All nonhydrogen atoms were refined with anisotropic displacement coefficients. All H atoms were found on the difference maps and refined with isotropic thermal parameters. All software and sources of scattering factors are contained in the SHELXTL (5.10) program package (G.Sheldrick, Bruker XRD, Madison, WI). Compound **1** was solved in space group *C*2/*c* with an R(F) = 6.9% with 28422 reflections measured. A complete crystal structure analysis can be found in the crystallographic information file (CIF) in the Supporting Information.

**Theoretical methods.** Geometries were optimized and vibrational analyses were performed at the density functional (DFT) level

(45) Chang, L. S.; Corey, J. Y. *Organometallics* **1989**, *8*, 1885–1893.
(46) Gilman, H.; Gaj, B. J. *J. Org. Chem.* **1957**, *22*, 447–449.
(47) Chen, J.; Law, C. C. W.; Lam, J. W. Y.; Dong, Y.; Lo, S. M. F.; Williams, I. D.; Zhu, D.; Tang, B. Z. *Chem. Mater.* **2003**, *15*, 1535–1546.
(48) Ruhlmann, K. *Z. Chem.* **1965**, *5*, 354.
(49) Liu, Y.; Stringfellow, T. C.; Ballweg, D.; Guzei, I. A.; West, R. *J. Am. Chem. Soc.* **2002**, *124*, 49–57.
(50) Dennis, J. W. H.; Rosenblatt, D. H.; Blucher, W. G.; Coon, C. L. *J. Chem. Eng. Data* **1975**, *20*, 202–203.

of theory using the 6–31G* basis set.[51] The hybrid B3LYP functional was employed, which combines Becke's gradient-corrected exchange functional[52] with gradient-corrected correlation functional of Lee, Yang, and Parr.[53] The vibrational analyses were used to confirm the nature of the stationary points, and the unscaled vibrational frequencies were used to compute thermal contributions to enthalpies. Excited-state energy calculations on **1a** and **2a** were carried out using TD-DFT methods on previously optimized ground-state structures.[54] All calculations were carried out with the Gaussian 03 suite of programs.[55]

**Solid-State Explosives Detection.** Solutions of the high explosives RDX, HMX, Tetryl, PETN, and TNG were prepared directly from dilute analytical standards purchased from Cerilliant. The explosive solutions were spotted onto Whatman filter paper at the desired concentration level using a glass microsyringe. A solvent blank was spotted next to each explosive as a control. All depositions were prepared from a 5 $\mu$L volume, producing a spot of ~1 cm in diameter, to ensure consistent analysis. Detection limits are reported in nanogram per square centimeter to emphasize the quantity of explosive materials deposited. Upon solvent evaporation, the substrate is airbrushed at a rate of 0.5 mL $s^{-1}$ with a 0.5 mg $mL^{-1}$ solution (1:1 toluene:acetone) of the desired polymer. The addition of toluene facilitates the transient dissolution of explosive analytes to ensure effective mixing with the polymers upon drying. Polymers **4** and **5** were visualized using a blacklight ($\lambda_{em}$ = 365 nm) as the excitation source and identified by their yellow-green luminescence. A blue luminescence was observed for polymer **6** using a UV-C light source ($\lambda_{em}$ = 254 nm). Similar detection limits for the high explosive analytes were observed using polymer **6** illuminated by a UV-B ($\lambda_{em}$ = 302 nm) light source. Detection studies were performed for each explosive at trace contamination levels of 64, 32, 16, 8, 3, 2, 1, 0.6, and 0.3 ng $cm^{-2}$. In the case of Tetryl, several dilutions were necessary in order to reach the detection limit.

Illuminated samples were examined by an independent observer to determine if quenching was visually discernible. A double-blind test was carried out using two spots of the explosive material at each concentration, which were spotted randomly onto three locations along with solvent blanks. The independent observer was unaware where the solvent control and explosive spots were distributed. Dark spots in the luminescent film indicate quenching of the polymer by the analyte. Detection limits are reported as the lowest amount of explosive necessary for the independent observer to observe quenching visually and accurately (>95%) in the correct locations. A summary of the detection limits is reported in Table 4. Different sampling surfaces, such as glass and porcelain, were also tested. Similar detection limits were observed for polymers **4** and **5** on these surfaces. Detection limits for polymer **6** decreased for the white porcelain surface. The smooth and shiny surface scattered the UV-C light, producing a reflection with a similar color as the emitting polymer. This affected the ability to observe quenching at low explosive concentrations. On filter paper, where reflected light was less problematic, polymer **6** had the lowest detection limits for all explosives studied.

**1,1-Diethynylsilafluorene (DESF).** To a dry THF solution of 1,1-dichlorosilafluorene (1.0 g, 4.0 mmol) was slowly added ethynylmagnesium bromide (0.5 M in THF, 16 mL, 8 mmol). The solution was stirred at room temperature for 2 h. The light brown solution was filtered and evaporated to dryness. The light brown solid was purified by sublimation (90–110 °C, 0.2 Torr) to afford a white crystalline solid (640 mg, 70%). Selected data. MP: 139–141 °C. $^1$H NMR (300.134 MHz, $CDCl_3$): $\delta$ 7.80 (dd, 4H, PhH), 7.50 (td, 2H, PhH), 7.35 (td, 2H, PhH); 2.60 (s, 2H, -C'CH). $^{13}$C{H} NMR (75.403 MHz, $CDCl_3$): $\delta$ 148.62, 133.83, 132.13, 131.60, 128.71, 121.49, 96.91, 82.04. $^{29}$Si NMR (71.548 MHz, inversed gated decoupling, $CDCl_3$): $\delta$ −51.2 (s, silafluorene). IR (KBr): $\nu_{C\equiv C}$ = 2028 $cm^{-1}$, $\nu_{\equiv C-H}$ = 3244 $cm^{-1}$. Calcd for $C_{16}H_{10}Si$: C, 80.3; H, 4.63; Found: C, 80.8; H, 4.43.

**1,1′-(1*E*,1′*E*)-2,2′-(2,3,4,5-tetraphenyl-1H-silole-1,1-diyl)bis(ethene-2,1-diyl)bis(1-methyl-2,3,4,5-tetraphenyl-1H-silole) (methyl(tetraphenyl)silole-vinylene trimer) (1).** To a dry toluene (8 mL) solution of 1,1-diethynyl(tetraphenyl)silole (200 mg, 0.46 mmol) and 1-methyl-1-hydrido(tetraphenyl)silole (378 mg, 0.92 mmol) was added $H_2PtCl_6$ (1 mg, 0.003 mmol). The solution was stirred at 70 °C for 3 h. The orange solution was then filtered and the solvent removed by vacuum. The brown residue was precipitated from 1 mL of THF with 10 mL of MeOH to afford a yellow powder (395 mg, 70%), which was recrystallized from benzene. Selected data. MP: 243–246 °C. $^1$H NMR (300.134 MHz, $CDCl_3$): $\delta$ 6.76–7.06 (br, 64H, PhH, −HC=CH−), 0.508 (s, 6H, $-CH_3$). $^{29}$Si NMR (71.548 MHz, inverse gated decoupling, $CDCl_3$): $\delta$ −2.66 (s, silafluorene). Calcd for $C_{90}H_{70}Si_3$: C, 87.5; H, 5.71. Found: C, 87.3; H, 6.04.

**5,5-bis((*E*)-2-(1-Methyl-2,3,4,5-tetraphenyl-1H-silol-1-yl)vinyl)-5H-dibenzo[b,d]silole (methyl(tetraphenyl)silole-silafluorene-vinylene cotrimer) (2).** To a dry toluene (8 mL) solution of **1** (150 mg, 0.65 mmol) and 1-methyl-1-hydrido(tetraphenyl)silole (522 mg, 1.3 mmol) was added $H_2PtCl_6$ (1 mg, 0.003 mmol). The solution was stirred at 70 °C for 3 h. The orange solution was then filtered and the solvent removed by vacuum. The brown residue was precipitated from 1 mL of THF with 10 mL of MeOH to afford a light yellow powder (430 mg, 64%). Selected data. MP: 120 °C (dec). $^1$H NMR (300.134 MHz, $CDCl_3$): $\delta$ 7.84 (dd, 4H, PhH), 7.45 (td, 2H, PhH), 6.76–7.06 (br, 46H, PhH, −HC=CH−), 0.502 (s, 6H, $-CH_3$). $^{29}$Si NMR (71.548 MHz, inversed gated decoupling, $CDCl_3$): $\delta$ −2.66 (s, silafluorene). Calcd for $C_{74}H_{58}Si_3 \cdot 2.0H_2O$: C, 83.3; H, 5.85. Found: C, 83.5; H, 6.03.

**5,5′-(1*E*,1′*E*)-2,2′-(5H-Dibenzo[b,d]silole-5,5-diyl)bis(ethene-2,1-diyl)bis(5-methyl-5H-dibenzo[b,d]silole) (Methylsilafluorene-Vinylene Trimer) (3).** To a dry toluene (8 mL) solution of **1** (150 mg, 0.65 mmol) and 1-methyl-1-hydridosilafluorene (256 mg, 1.3 mmol) was added $H_2PtCl_6$ (1 mg, 0.003 mmol). The solution was stirred at 50 °C for 2 h. The orange solution was then filtered and the solvent removed under vacuum. The brown residue was precipitated from 1 mL of THF with 10 mL of MeOH to afford a white powder (270 mg, 66%). Selected data.

(51) Hariharan, P. C.; Pople, J. A. *Theor. Chim. Acta* **1973**, *28*, 213–222. Several calculations at the B3LYP/6–311+G** level of theory for **1** and **3** show that the extra valence and diffuse functions give results similar to those of the 6–31G* basis set used in this study.
(52) Becke, A. D. *J. Chem. Phys.* **1993**, *98*, 5648–5652.
(53) Lee, C.; Yang, W.; Parr, R. G. *Phys. Rev. B* **1988**, *37*, 785–789.
(54) (a) Stratmann, R. E.; Scuseria, G. E.; Frisch, M. J. *J. Chem. Phys.* **1998**, *109*, 8218–8224. (b) Bauernschmitt, R.; Ahlrichs, R. *Chem. Phys. Lett.* **1996**, *256*, 454–464. (c) Casida, M. E.; Jamorski, C.; Casida, K. C.; Salahub, D. R. *J. Chem. Phys.* **1998**, *108*, 4439–4449.
(55) Frisch, M. J.; Trucks, G. W.; Schlegel, H. B.; Scuseria, G. E.; Robb, M. A.; Cheeseman, J. R.; Montgomery Jr., J. A.; Vreven, T.; Kudin, K. N.; Burant, J. C.; Millam, J. M.; Iyengar, S. S.; Tomasi, J.; Barone, V.; Mennucci, B.; Cossi, M.; Scalmani, G.; Rega, N.; Petersson, G. A.; Nakatsuji, H.; Hada, M.; Ehara, M.; Toyota, K.; Fukuda, R.; Hasegawa, J.; Ishida, M.; Nakajima, T.; Honda, Y.; Kitao, O.; Nakai, H.; Klene, M.; Li, X.; Knox, J. E.; Hratchian, H. P.; Cross, J. B.; Bakken, V.; Adamo, C.; Jaramillo, J.; Gomperts, R.; Stratmann, R. E.; Yazyev, O.; Austin, A. J.; Cammi, R.; Pomelli, C.; Ochterski, J. W.; Ayala, P. Y.; Morokuma, K.; Voth, G. A.; Salvador, P.; Dannenberg, J. J.; Zakrzewski, V. G.; Dapprich, S.; Daniels, A. D.; Strain, M. C.; Farkas, O.; Malick, D. K.; Rabuck, A. D.; Raghavachari, K.; Foresman, J. B.; Ortiz, J. V.; Cui, Q.; Baboul, A. G.; Clifford, S.; Cioslowski, J.; Stefanov, B. B.; Liu, G.; Liashenko, A.; Piskorz, P.; Komaromi, I.; Martin, R. L.; Fox, D. J.; Keith, T.; Al-Laham, M. A.; Peng, C. Y.; Nanayakkara, A.; Challacombe, M.; Gill, P. M. W.; Johnson, B.; Chen, W.; Wong, M. W.; Gonzalez, C.; Pople, J. A. *Gaussian 03*, revision B.05; Gaussian, Inc.: Wallingford, CT, 2004.

MP: 70 °C (dec). $^1$H NMR (300.134 MHz, $CDCl_3$): $\delta$ 7.81 (br, 12H, PhH), 7.56 (br, 6H, PhH), 7.42 (br, 6H, PhH), 6.80 (dd, 4H, −HC=CH−, $J$ = 22 Hz), 0.472 (s, 6H, $-CH_3$). $^{29}$Si NMR (71.548 MHz, inversed gated decoupling, $CDCl_3$): $\delta$ 1.18 (center Si), −9.44 (endgroups).Calcd for $C_{42}H_{34}Si_3 \cdot H_2O$: C,78.7; H, 5.66. Found: C, 79.1; H, 5.93.

**Poly(tetraphenylsilole-vinylene) (PSV) (4).** To a dry toluene (3 mL) solution of 1,1-diethynyl(tetraphenyl)silole (100 mg, 0.23 mmol) and 1,1-dihydrido(tetraphenyl)silole (89 mg, 0.23 mmol) was added $H_2PtCl_6$ (1 mg, 0.003 mmol). The solution was stirred at 80 °C for 24 h. The orange solution was filtered and the solvent removed by vacuum evaporation. The brown residue was precipitated from 1 mL of THF with 10 mL of MeOH to afford a yellow powder (138 mg, 73%). Selected data. $^1$H NMR (300.134 MHz, $CDCl_3$): $\delta$ 6.20–8.10 (br, PhH, −HC=CH−), 2.61 (s, 2H, −C≡C−H, terminal). $^{29}$Si NMR (71.548 MHz, inversed gated decoupling, $CDCl_3$): $\delta$ 6.0 (weak signal). Calcd for $C_{30}H_{22}Si \cdot 1.5H_2O$: C, 82.4; H, 5.76. Found: C, 82.9; H 5.78.

**Poly(tetraphenylsilole-silafluorene-vinylene) (5).** To a dry toluene (3 mL) solution of **1** (100 mg, 0.43 mmol) and 1,1-dihydrido(tetraphenyl)silole (168 mg, 0.43 mmol) was added $H_2PtCl_6$ (1 mg, 0.003 mmol). The solution was stirred at 80 °C for 24 h. The orange solution was then filtered and the solvent removed under vacuum. The brown residue was precipitated from 1 mL of THF with 10 mL of MeOH to afford a light yellow powder (190 mg, 71%). Selected data. $^1$H NMR (300.134 MHz, $CDCl_3$): $\delta$ 5.60–8.20 (br, PhH, −HC=CH−), 2.56 (s, 2H, −C≡CH, terminal). $^{29}$Si NMR (71.548 MHz, inversed gated decoupling, $CDCl_3$): $\delta$ 6.0 (weak signal). Calcd for $C_{44}H_{32}Si_2 \cdot H_2O$: C, 83.3; H, 5.40. Found: C, 83.4; H, 5.94.

**Poly(silafluorene-vinylene) (PSFV) (6).** To a dry toluene (3 mL) solution of **1** (100 mg, 0.43 mmol) and 1,1-dihydridosilafluorene (79 mg, 0.43 mmol) was added $H_2PtCl_6$ (1 mg, 0.003 mmol). The solution was stirred at 80 °C for 24 h. The orange solution was then filtered and the solvent removed under vacuum. The brown residue was precipitated from 1 mL of THF with 10 mL of MeOH to afford a yellow powder (118 mg, 66%). Selected data. $^1$H NMR (300.134 MHz, $CDCl_3$): $\delta$ 5.80–8.50 (br, PhH, −HC=CH−), 2.55 (s, 2H, −C≡CH, terminal). $^{29}$Si NMR (71.548 MHz, inverse gated decoupling, $CDCl_3$): $\delta$ 6.0 (weak signal); CH calcd for $C_{13}H_{10}Si \cdot 0.5H_2O$: C, 76.7; H, 5.45. Found: C, 77.2; H, 5.09.

**1-Methyl-1-vinyl(tetraphenyl)silole (7).** Diphenylacetylene (10 g, 56 mmol) and chopped lithium wire (62 mmol) in dry THF (40 mL) were stirred overnight under argon. The dark green reaction was cannulated into a solution of methylvinyldichlorosilane (4 mL, 31 mmol) and dry THF (90 mL) and stirred for 2 h at room temperature and then refluxed for 5 h. The reaction was quenched with sat. $NH_4Cl$ and the organic solvent was removed by evaporation under vacuum. Extraction and crystallization in ether afforded yellow crystals (6.9 g, 59%). Selected data. MP: 73–74 °C (Lit: 77–78 °C).[56] $^1$H NMR (300.133 MHz, $CDCl_3$): $\delta$ 6.80–7.15 (br. m, 20H, PhH), 6.37 (dd, 1H, SiCH=C), 6.19 (dd, 1H, $-C=CH_2$), 5.97 (dd, 1H, $-C=CH_2$), 0.589 (s, 3H, $-CH_3$). $^{13}$C{H} NMR (75.403 MHz, $CDCl_3$): $\delta$ 155.34, 140.23, 139.73, 139.04, 136.38, 133.86, 130.17, 129.25, 128.12, 127.71, 126.53, 125.87, −6.34. $^{29}$Si NMR (99.36 MHz, INEPT, $CDCl_3$, TMS ($\delta$ 0.0)): $\delta$ −1.95 (s, silole). Calcd for $C_{31}H_{26}Si$: C, 87.2; H, 6.14. Found: C, 87.1; H, 6.24.

**1-Methyl-1-vinylsilafluorene (8).** To a dry ethereal solution of 2,2′-dibromobiphenyl (5.0 g, 16 mmol) was slowly added *n*-BuLi (1.6 M in hexanes, 21 mL, 33 mmol) at −78 °C. The solution was stirred at −78 °C for 10 min and then at room temperature overnight. To the cloudy yellow-green solution was added methylvinyldichlorosilafluorene (2.08 mL, 16 mmol) at −78 °C. The solution was stirred for 20 min and then stirred overnight at room temperature. The cloudy white reaction mixture was quenched with $NH_4Cl$ and extracted with ether. The organics were dried over $MgSO_4$ and evaporated to dryness. The light yellow solid was recrystallized in hexanes to afford white crystals (1.8 g, 51%). Selected data. MP: 58–60 °C. $^1$H NMR (300.134 MHz, $CDCl_3$): $\delta$ 7.85 (d, 2H, PhH), 7.64 (d, 2H, PhH), 7.46 (t, 2H, PhH), 7.30 (t, 2H, PhH), 6.26 (dd, 1H, SiCH=), 6.15 (dd, 1H, $=CH_2$), 5.97 (dd, 1H, $=CH_2$), 0.542 (s, 3H, $-CH_3$). $^{13}$C{H} NMR (75.403 MHz, $CDCl_3$): $\delta$ 148.49, 137.41, 135.53, 134.31, 133.45, 130.65, 127.73, 121.18, −5.46. $^{29}$Si NMR (71.548 MHz, inverse gated decoupling, $CDCl_3$): $\delta$ −8.52 (s, silafluorene). Calcd for $C_{15}H_{14}Si$: C, 81.0; H, 6.35. Found: C, 80.9; H, 6.81.

**Acknowledgment.** This work was supported by the Air Force Office of Scientific Research (AFOSR-MURI F49620-02-1-0288) and the National Science Foundation (NSF-GRFP).

**Supporting Information Available:** Crystallographic information (CIF) for compound **1**. $^1$H NMR spectra for DESF and compounds **1**−**3**, **7**, and **8**; tabulated HOMO and LUMO energies for the explosives used in this study at the B3LYP/6–311+G** level of theory; frontier orbital density diagrams for TNT, RDX, HMX, PETN, **1**, and **3** (PDF). This material is available free of charge via the Internet at http://pubs.acs.org.

CM702299G

(56) Balasubramanian, R.; George, M. V. *Tetrahedron* **1973**, *29*, 2395–2404.